ELSEVIER

Surface Science 425 (1999) 296–312

surface science

Adsorption and disproportionation reaction of OH on Ag surfaces: dipped adcluster model study

Zhen-Ming Hu [a], Hiroshi Nakatsuji [a,b,*]

[a] *Department of Synthetic Chemistry and Biological Chemistry, Graduate School of Engineering, Kyoto University, Sakyo-ku, Kyoto, 606-8501, Japan*

[b] *Institute for Fundamental Chemistry, 34-4 Takano-Nishihiraki-cho, Sakyo-ku, Kyoto 606, Japan*

Received 26 August 1998; accepted for publication 22 January 1999

Abstract

The adsorption and surface disproportionation reactions of OH on various silver surfaces were studied by the dipped adcluster model (DAM) combined with ab initio HF and MP2 methods. Our studies show that OH binds strongly to Ag surfaces; the adsorption energies were calculated to be 118.3 kcal mol^{-1} at the short bridge site on Ag(110), 108.6 kcal mol^{-1} at the fourfold hollow site on Ag(100), and 97.3 kcal mol^{-1} at the threefold hollow site on Ag(111). The H–O axis is preferentially perpendicular to the surface for OH on Ag(100) and Ag(111), but tilts about 50° along the [001] azimuthal orientation on Ag(110). The Ag 4d orbital plays an important role in adsorbing OH, whose molecular orbital analysis is described. Coadsorption of OH at the nearest fourfold sites on Ag(100) is stable with the H–O axis perpendicular to the surface; an inclined OH structure is proposed for the coadsorption of OH at the bridge sites and it is shown to be very reactive regarding the surface disproportionation reaction of OH. The structures and energy surfaces for the disproportionation reaction of OH to form H_2O on Ag(100) are presented. The present study provides clear information regarding the adsorption, coadsorption and disproportionation of OH on Ag surfaces.

Keywords: Ab initio quantum chemical methods and calculations; Catalysis; Chemisorption; Hydroxyl; Metallic surface; Models of surface chemical reactions; Silver; Surface chemical reaction

1. Introduction

The adsorption and disproportionation of hydroxyl radicals on metal surfaces have recently been the subject of considerable experimental and theoretical examination since they are of fundamental importance in heterogeneous catalysis, electrochemistry and corrosion. Hydroxyl radicals are formed in the oxidation of hydrogen and hydrocarbons [1], and in the water-gas shift reaction [2]. Experimentally, information about the adsorption behavior of OH can be obtained by studying the interaction of H_2O with preadsorbed oxygen on metal surfaces. This reaction can be described as

$$H_2O + O(a) \rightarrow 2OH(a). \quad (1)$$

The adsorbed OH species can recombine to produce H_2O via disproportionation at a higher temperature:

$$2OH(a) \rightarrow H_2O + O(a). \quad (2)$$

There have been several investigations of OH

* Corresponding author. Fax: +81 75-753-5910.
E-mail address: a5032@jpnkudpc (Hiroshi Nakatsuji)

0039-6028/99/$ – see front matter
PII: S0039-6028(99)00215-0

adsorbed on the surfaces of transition metals such as Ni [3–6], Pd [6–8], Ru [9,10], Pt [11–16], Rh [6,17], etc. Compared with transition metal surfaces, only limited information is available regarding the noble metals Cu [18–20] and Ag [20–24]. On the other hand, despite numerous efforts, little quantitative experimental work has been published on OH adsorption on well-characterized metal surfaces, perhaps due to the problem of clearly identifying surface OH in the presence of other coadsorbates.

Silver is an important catalyst in industrial processes such as the epoxidation of ethylene [25] and the production of aldehyde from alcohol [26]. The interaction of OH with an Ag surface is of considerable fundamental and practical interest since it acts as a reaction intermediate in these catalytic processes. Experimental data are available for OH adsorption on Ag(111) [20,21], Ag(100) [21] and Ag(110) [22–24] surfaces. Klaua and Madey [21] studied the interaction of H_2O with oxygen-covered silver surfaces. They found that the interaction of H_2O with preadsorbed O at 80 K does not result in azimuthal ordering of adsorbed H_2O on any of the Ag facets, in marked contrast to the local ordering observed for H_2O+O on Ni(111) [5]. Adsorbed H_2O reacts with preadsorbed oxygen to form OH species that are bonded with the molecular axis perpendicular to Ag(111) and Ag(100), as shown using electron-stimulated desorption ion angular distribution (ESDIAD) [21]. The OH species form an ordered $c(2\times2)$ overlayer on Ag(100), while there is no evidence of ordered OH low energy electron diffraction (LEED) structures for Ag(111). The $c(2\times2)$ LEED pattern disappeared after heating to 300 K, but reappeared after redosing with H_2O and heating to 160 K [21].

Ordered $(1\times m)$ $(m=1, 2, 3)$ LEED patterns of OH on Ag(110) surfaces were reported by Bange et al. [22] and Canepa et al. [24]. Bange et al. [22] proposed that OH is coordinated to three Ag atoms with a local (111) structure. In their LEED and ESDIAD studies, the O–H bond axis is tilted with respect to the surface normal and the azimuthal orientation is along the [001] direction [22]. On the other hand, Canepa et al. [24] proposed an adsorption site with C_{2v} symmetry in the (1×2) and (1×3) patterns on Ag(110) by metastable de-excitation spectroscopy (MDS) and angle-resolved UPS (ARUPS) studies. Adsorption of OH leads to a noticeable variation in the spectra. An important change involves the feature in the 10–14 eV region that may be assigned to OH 3σ, and two other features around 8 eV associated with OH 1π orbitals [24]. However, both Bange et al. [22] and Canepa et al. [24] pointed out that the exact geometry of OH on Ag surfaces has yet to be determined, and a better understanding could be achieved by both further measurements and model calculations.

On the theoretical side, several studies have examined the adsorption of OH on Pt(111) [27], Fe(100) [27], Ni(100) [28,29], Ni(111) [29–31], Cu(111) [32] and Ag(111) [33] surfaces. A semi-empirical calculation for OH adsorption on Pt and Fe surfaces performed by Anderson [27] showed that the interactions of OH with metal surfaces are due to the mixing of OH 1π with metal d states, leading to bonding and anti-bonding below and above the metal d bands respectively. OH binds strongly to a clean metal surface and is preferentially adsorbed at high-coordination sites in Ni(100) [29], Ni(111) [29–31] and Cu(111) [32]. The valence orbital structure of hydroxyl is characterized by partially filled 1π orbitals, which are similar in shape and energy to the O 2p states. Chemisorption of OH on metal surfaces is generally interpreted in terms of bonding via the oxygen atom with a charge transfer from the surface to the 1π orbitals.

In our previous studies [34–36], a theoretical model, called the dipped adcluster model (DAM), has been proposed to study chemisorptions and surface reactions involving electron transfer between admolecules and surfaces. The DAM has been successfully applied to harpooning, surface chemiluminescence and electron emission in the halogen–alkali-metal surface system [37], and to the study of oxygen chemisorption on an Ag surface [38–40]. Most recently, the mechanisms of the epoxidation and complete oxidation of ethylene [41–43] and propylene [43,44] on a silver surface have been clarified using the DAM. The uniqueness of the silver surface for ethylene epoxidation has been clarified by a comparative study of the

stability and activity of oxygen species on Cu, Ag, and Au surfaces [45]. The mechanism of the hydrogenation of CO_2 to methanol over a Cu(100) surface has also been clarified [46].

In this paper, we provide for the first time an ab initio theoretical study of the adsorption and disproportionation of OH on silver surfaces using the DAM combined with the ab initio Hartree–Fock (HF) and second-order Møller–Plesset (MP2) calculations. We are mainly interested in clarifying the adsorption behavior of OH, and the mechanism of the surface disproportionation reaction of $2OH \rightarrow H_2O + O$ on Ag surfaces. Section 2 presents an outline of the computational details. In Section 3 we present numerical results and discuss OH adsorption on Ag(100), Ag(111), and Ag(110) surfaces. In Section 4 we discuss the coadsorption of OH + OH on Ag(100). In Section 5 we study the structures and energy surfaces for the surface disproportionation of $2OH \rightarrow H_2O + O$ on an Ag(100) surface. Concluding remarks are provided in Section 6.

2. Computational details

The clusters used to simulate the Ag(100), Ag(110), and Ag(111) surfaces are shown in Fig. 1. The Ag(100) surface is simulated by an $Ag_8(6,2)$ cluster, which contains six silver atoms in the first layer and two silver atoms in the second layer. An $Ag_{11}(8,3)$ cluster is then used to check the cluster size dependence for OH adsorption and coadsorption, and to study the disproportionation reaction of OH at the bridge sites on an Ag(100) surface. The Ag(110) surface is simulated by an $Ag_{10}(4,6)$ cluster, which contains four silver atoms in the first layer and six silver atoms in the second layer. An $Ag_{10}(10,0)$ cluster, which has ten silver atoms in the first layer, is used to simulate the Ag(111) surface. The positions of the atoms in the cluster are distinguished by the Albanian number. The sites considered for OH adsorption are also depicted in Fig. 1 by the small filled circles. The electronic states of the clusters are determined by the ab initio MP2 method using the Gaussian-type basis set given below. The ionization energies by Koopmans' theorem are calculated to be

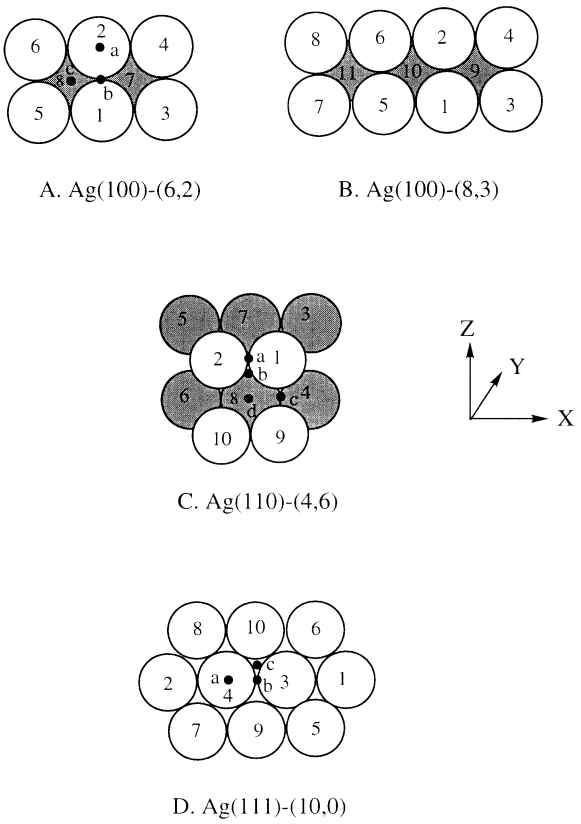

Fig. 1. Geometric structures of the clusters used to model the Ag(100), Ag(110) and Ag(111) surfaces. The first layer of silver atoms is denoted by open circles (○) and the second layer is denoted by shaded circles (◍). The small filled circles (●) denote adsorption sites. (a) The on-top, bridge and fourfold hollow sites on the Ag(100)-(6,2) surface. (b) The short-bridge, threefold, long-bridge and fourfold on-top sites on the Ag(110)-(4,6) surface. (c) The on-top, bridge and threefold hollow sites on the Ag(111)-(10,0) surface.

4.61 eV, 4.33 eV, and 4.97 eV for Ag(100), Ag(110), and Ag(111) respectively, which are comparable to the experimental values of the Ag(100), Ag(110), and Ag(111) work functions [47] (4.61 eV, 4.52 eV, and 4.74 eV respectively).

Electron exchange between the adcluster and the bulk metal is taken into account by the DAM [33–36]. The calculations were performed using the highest spin coupling model [37] and so one electron transfer from a bulk metal was assumed, namely the adcluster with one negative charge is considered [37–40]. Electrostatic interaction

between the admolecule and the extended surface is estimated by the image force correction [35]. All of the geometries are optimized by the energy gradient method at the HF level except for the Ag–Ag distance, which is fixed at its bulk lattice value of 2.8894 Å. The electron correlations are considered by the MP2 method. Some calculational details are illustrated in the corresponding text. The energy scale is in kilocalories per mole, and the bond distances and bond angles are given in Ångströms and degrees respectively. The calculations were performed using the Gaussian 94 software package [48].

The Gaussian basis set for the silver atom is (3s3p4d)/[3s2p1d] and the Kr core was replaced by the effective core potential [49]. For oxygen, we use the (9s5p)/[4s2p] set of Huzinaga–Dunning [50,51] augmented by the diffuse s and p functions of $\alpha=0.059$ [52] and the polarization d function of $\alpha=1.154$ [53]. For hydrogen, (4s)/[2s] augmented by the polarization p function of $\alpha=1.0$ is adopted [52]. The basis sets are similar to those used in our previous studies [41–46].

3. Adsorption of OH on silver surfaces

In this section we study the adsorption of OH on Ag(100), Ag(110), and Ag(111) surfaces. The geometries of the adsorbed OH species are in all cases optimized by the energy gradient method at the HF level. The OH molecular axis is initially assumed to be perpendicular to the surface, and the effect of tilting the O–H axis away from the surface normal is examined to elucidate the local adsorption geometry. The adsorption energies are relative to the free OH and Ag cluster, and are calculated by the MP2 method. The HO–surface stretching frequencies are calculated using a one-dimensional harmonic oscillator model.

3.1. OH adsorption on Ag(100)

Table 1 shows the calculated adsorption energies, optimized geometries and HO–surface stretching frequencies for OH adsorbed at different sites on an Ag(100) surface. The OH molecular axis is assumed to be perpendicular to the surface. OH adsorption at the fourfold hollow site is found to be the most stable. The calculated adsorption energy is 108.3 kcal mol^{-1} with an O–surface perpendicular distance of 1.46 Å. Adsorptions at the on-top and bridge sites are calculated to be less stable by 11 kcal mol^{-1} and 6 kcal mol^{-1} respectively. The relative stabilities are the same as those reported for OH adsorbed on Ni(100) [29]. The HO–surface stretching frequencies are calculated to be 368 cm^{-1}, 299 cm^{-1} and 243 cm^{-1} for the on-top, bridge and fourfold hollow adsorption sites respectively, at the optimized geometry with the H–O axis normal to the surface. The energies and geometries calculated by using the Ag_{11} cluster are also shown in Table 1 (in parentheses). The results are similar to those on the Ag_8 cluster, and are almost convergent with the cluster size.

To elucidate the local adsorption geometry, in

Table 1
Adsorption energies, optimized geometries and HO–surface stretching frequencies for OH adsorbed at different sites on Ag(100) surface

Site[a]	E_{ads} (kcal mol^{-1})[b]	$R_{O-surface}$ (Å)[c]	R_{O-Ag} (Å)[c]	R_{O-H} (Å)[c]	HO–Ag stretch (cm^{-1})
On-top	97.2	2.137	2.137	0.94	368
Bridge	102.3 (101.4)	1.803 (1.789)	2.310 (2.30)	0.94 (0.94)	299
Fourfold	108.6 (109.9)	1.464 (1.456)	2.513 (2.51)	0.95 (0.95)	243

[a] Adsorption sites are illustrated in Fig. 1a.

[b] Adsorption energy is defined as $E_{ads}=-[E(Ag_8OH)-E(Ag_8)-E(OH)]$ and calculated by the MP2 method. Positive values are exothermic.

[c] $R_{O-surface}$ is the perpendicular distance from oxygen to the Ag surface, and R_{O-Ag} is the corresponding distance from the oxygen nucleus to the nearest Ag nucleus. All the geometries are calculated by an HF optimization procedure except the assumption that the H–O molecular axis is perpendicular to the surface normal. The results calculated using the Ag_{11} cluster are given in parentheses.

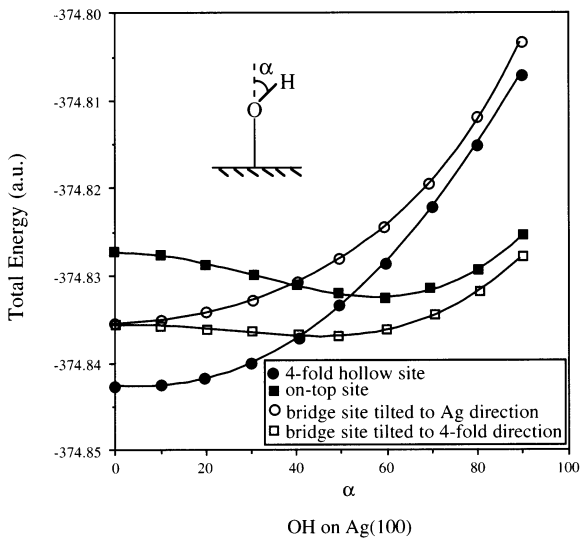

Fig. 2. Potential energy as a function of the angle α between the H–O axis and the surface normal for OH on Ag(100). Definitions are also given in the text.

Fig. 2 we show the calculated potential energy curve as a function of the angle α between the H–O axis and the surface normal. The geometries with minimum energy were $\alpha = 0^\circ$, 50° and 60° at the fourfold hollow, bridge and on-top sites respectively. Interestingly, at the bridge site, the total energy increases when the H–O axis is tilted in the direction of the nearest silver atom, while the energy decreases by about 2.0 kcal mol^{-1} when this axis is tilted about 50° in the direction of the fourfold hollow site. This difference may reflect the dependence of the reactivity of the adsorbed OH at the bridge site on its orientation, as discussed below. At the on-top site, the total energy is reduced by 3.1 kcal mol^{-1} when the H–O axis is tilted about 60° toward the surface normal. Our results support the experimental findings [21] that, for OH on Ag(100), the most stable geometry is OH adsorbed at the fourfold hollow site with its molecular axis perpendicular to the surface normal. This result for OH at the fourfold site is similar to that for OH adsorbed on Ni(100) [29]; however, for OH at the bridge site, only a perpendicular geometry has been reported on Ni(100) [29].

Table 2 shows the calculated Mulliken charges

Table 2
Mulliken charges for OH adsorbed at different sites on the Ag(100) surface[a]

No.	Atom	Free species	On-top	Bridge	Fourfold
1	Ag	0.0226	0.0677	0.0855	0.0083
2	Ag	0.0226	0.3101	0.0855	0.0083
3	Ag	−0.0040	−0.1251	−0.0882	−0.0650
4	Ag	−0.0040	−0.0286	−0.0882	−0.0650
5	Ag	−0.0040	−0.1251	−0.0882	−0.1361
6	Ag	−0.0040	−0.0286	−0.0882	−0.1361
7	Ag	−0.0147	−0.1391	−0.0915	−0.0709
8	Ag	−0.0147	−0.1391	−0.0915	−0.1204
9	O	−0.3278	−1.0885	−0.9484	−0.7481
10	H	0.3278	0.2965	0.3133	0.3250

[a] The Ag(100) surface is simulated by an $Ag_8(6,2)$ cluster shown in Fig. 1a, and the adsorption sites are also illustrated in Fig. 1a. Mulliken charges are given relative to neutral atoms.

for the OH on Ag(100). Although a Mulliken population analysis to apportion the density in a chemical bond to its representative atoms is somewhat arbitrary, the results listed in Table 2 provide an approximate qualitative measure of charge and charge transfer. The strong interactions of OH with silver involve electron transfer from the surface to OH. The net charge transfer is calculated to be 0.79*e*, 0.64*e* and 0.42*e* for OH adsorbed at the on-top, bridge and fourfold hollow sites respectively.

Fig. 3 shows the orbital correlation diagram for OH at the bridge site on Ag(100); this is an example to show the bonding mechanism for OH on silver surfaces. The orbital levels shift dramatically in the adsorption state. The main OH 3σ bonding feature shifts from 18.08 to 12.90 eV, and the main OH 1π bonding features shift from 15.91 to 7.25 eV and from 15.30 to 6.99 eV. The orbital levels of OH at different sites on Ag(100), Ag(110), and Ag(111) surfaces are shown in Table 3. Experimentally, Canepa et al. [24] reported that the σ-bonding and π-bonding levels of OH are shifted to 10–14 eV and around 8 eV respectively by the adsorption on Ag(110). A detailed molecular orbital (MO) analysis shows that, in the bridge adsorption state, the OH 1π orbital (mainly the O $2p_y$ component) mixes strongly with Ag 4d states and to a lesser extent with 5s states, leading to bonding and anti-bonding

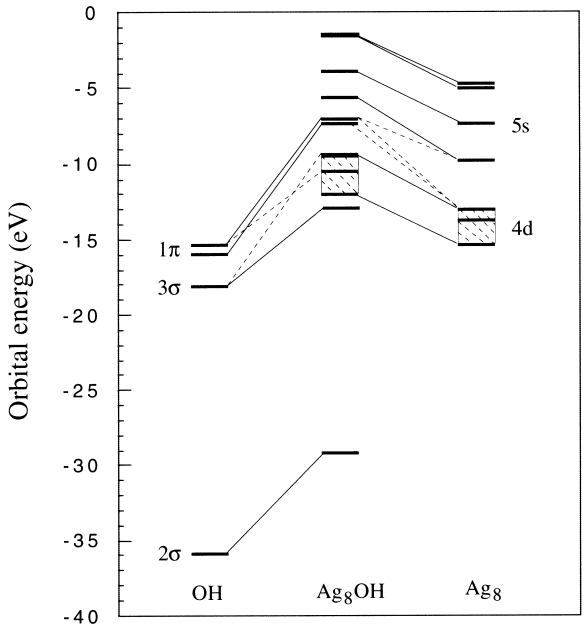

Fig. 3. Orbital correlation diagrams for the orbital interactions between the Ag 5s and 4d and OH 1π and 3σ orbitals for OH adsorbed at the short-bridge site on Ag(100) modeled by Ag_8. The solid lines show main contributions, and the dashed lines minor contributions to the MOs of Ag_8OH.

levels among and above the metal d bands respectively. Another OH 1π orbital (mainly the O $2p_x$ component) almost retains a non-bonding nature, as in the free state. The OH 3σ orbital (mainly the O $2p_z$ component) also mixes strongly with Ag 4d states, leading to bonding and anti-bonding levels below and above the metal d bands respectively. Such bonding interactions can be easily understood by the contour plots for the corresponding MOs, as shown in Fig. 4, in which the perpendicular H–O axis is taken as the z axis and the Ag_1–Ag_2–O molecular plane is taken as the yz plane. The same bonding and anti-bonding interactions are also found for OH at other sites and on other silver surfaces. The Ag 4d orbital plays an important role in the adsorption interaction with OH. Such orbital interactions lead to charge transfer from the Ag 5s and 4d orbitals to the partially vacant highest-lying anti-bonding 1π orbital of OH, and to charge transfer from OH back to the surface through the 3σ bonding orbital to Ag 4d. The latter is smaller than the former, leading to a net charge transfer from the surface to OH.

The orbital pictures presented here provide theoretical evidence for OH adsorption on Ag surfaces, and show some differences from that of OH adsorption on transition metal surfaces such as Pt(111) [27], Fe(100) [27] and Ni(111) [29–31]. The calculations for OH adsorption on Pt(111) [27] and Fe(100) [27] showed that the OH 3σ orbital does not mix with the metal d states and is much more stable in the adsorption states, whereas the 1π orbitals mix with the metal d, leading to bonding and anti-bonding levels below and above the metal d bands. The bonding nature of OH on Ag surfaces is similar to that of OH on Ni surfaces [29]; however, the OH 3σ orbital mixes only slightly with Ni 3d orbitals [30].

3.2. OH adsorption on Ag(110)

Table 4 shows the calculated adsorption energies, optimized geometries and HO–surface stretching frequencies for OH adsorbed at different sites on an Ag(110) surface. The calculated

Table 3
Molecular orbital levels (electron-volts) of OH at the free and adsorption states on Ag(100), Ag(111), and Ag(110)

Orbitals	OH (free)	OH on Ag(100)			OH on Ag(111)			OH on Ag(110)	
		on-top	bridge	hollow	on-top	bridge	hollow	s-bridge	hollow
1σ	561.50	552.55	553.17	554.45	551.86	553.23	553.63	553.71	554.40
2σ	35.82	28.45	29.14	30.30	27.72	29.21	29.59	29.77	30.58
3σ	18.08	12.56	12.90	13.65	12.31	13.18	13.45	13.68	14.37
1π	15.91	6.63	7.25	8.07	6.04	7.34	7.53	7.67	8.24
	15.30	6.54	6.99	7.97	6.01	7.16	7.47	7.35	8.19

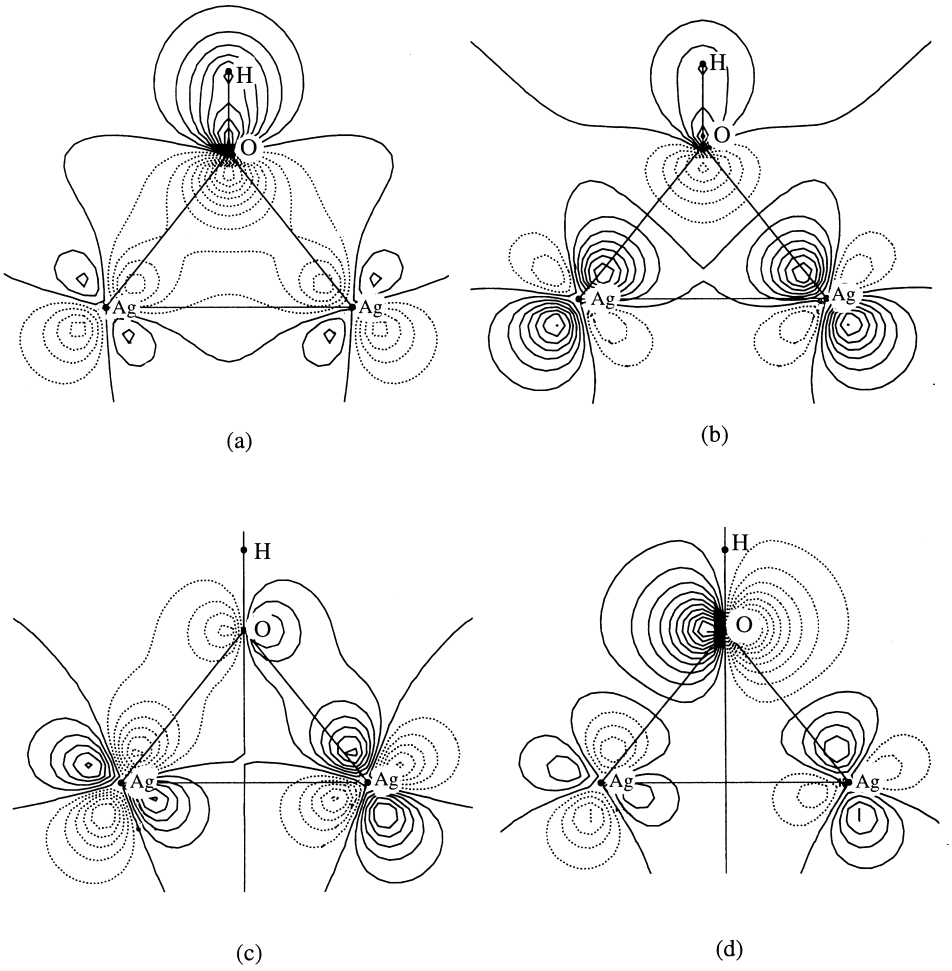

Fig. 4. Contour plots of MOs for OH adsorbed at the bridge site on an Ag(100) surface. (a) Bonding interaction of OH 3σ with Ag 4d; (b) anti-bonding interaction of OH 3σ with Ag 4d; (c) bonding interaction of OH 1π with Ag 4d; (d) anti-bonding interaction of OH 1π with Ag 4d. The contour value difference is ±0.05. The H–O axis is taken as the *z* axis, and only the plots at the Ag_1–Ag_2–O–H plane, which is taken as the *yz* plane, are shown.

adsorption energies are 118.3 kcal mol^{-1}, 105.6 kcal mol^{-1}, 104.5 kcal mol^{-1} and 99.4 kcal mol^{-1} for OH adsorbed at the short-bridge, threefold, long-bridge and fourfold on-top sites with O–Ag nearest distances of 2.23 Å, 2.35 Å, 2.43 Å and 2.64 Å respectively. The corresponding O–surface perpendicular distances are also listed in Table 4. The HO–surface stretching frequencies are calculated to be 335 cm^{-1}, 259 cm^{-1}, 193 cm^{-1} and 165 cm^{-1} for OH adsorbed at the short-bridge, threefold, long-bridge and fourfold on-top sites respectively. The experimental value of 280 cm^{-1} is reported for OH on Ag(110) [23]. In contrast to OH adsorption on Ag(100) and Ag(111) surfaces, the stability of the adsorbed OH decreases as the distance between O and the nearest Ag increases. The calculated potential surfaces at the fourfold on-top and bridge sites are very flat, leading to small HO–surface vibrational frequencies. The most stable site for OH on Ag(110) is calculated to be the short-bridge site, which is consistent with the ARUPS experimental C_{2v} symmetry site on Ag(110) reported by Canepa et al. [24], but different from the results of ESDIAD

Table 4
Adsorption energies, optimized geometries and HO–surface stretching frequencies for OH adsorbed at different sites on the Ag(110) surface

Site[a]	E (kcal mol^{-1})[b]	$R_{O-surface}$ (Å)[c]	R_{O-Ag} (Å)[c]	R_{O-H} (Å)[c]	HO–Ag stretch (cm^{-1})
On-top	99.4	1.200	2.644	0.942	165
Short-bridge	118.3	1.695	2.227	0.939	335
Long-bridge	104.5	1.317	2.431	0.941	193
Threefold	105.6	0.867	2.347	0.945	259
Experiment	–	–	–	–	280

[a] Adsorption sites are illustrated in Fig. 1a.
[b] Adsorption energy is defined as $E_{ads} = -[E(Ag_{10}OH) - E(Ag_{10}) - E(OH)]$ and calculated by the MP2 method. Positive values are exothermic.
[c] $R_{O-surface}$ is the perpendicular distance from oxygen to the Ag surface, and R_{O-Ag} is the corresponding distance from the oxygen nucleus to the nearest Ag nucleus. All the geometries are calculated by an HF optimization procedure except the assumption that the H–O molecular axis is perpendicular to the surface normal.

studies reported by Bange et al. [22] who suggested the threefold adsorption site for OH on Ag(110). Our calculations show that the threefold site is the second candidate, and is 13 kcal mol^{-1} less stable than the short-bridge site.

To elucidate the orientation of the O–H axis, the potential energy curve for OH adsorbed at the most stable short-bridge site was investigated and is shown in Fig. 5. Tilting of the H–O axis along the [110] azimuthal orientation increases the total energy, whereas it decreases by 2.7 kcal mol^{-1} when this axis is tilted about 50° along the [001] azimuthal direction. These results support the experimental result of Bange et al. [22] that the O–H bond axis is tilted toward the surface, and the azimuthal orientation is in the [001] direction.

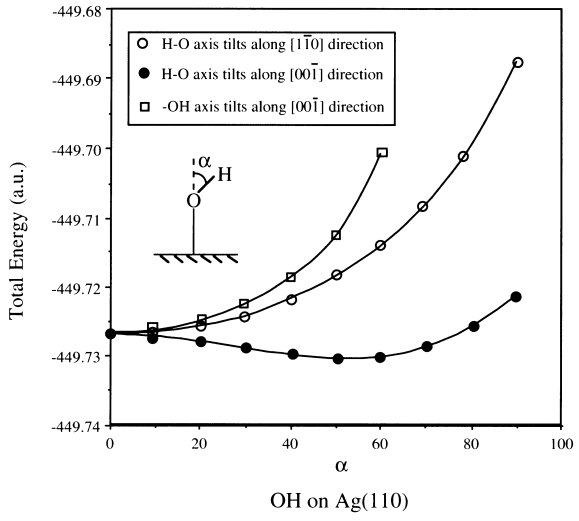

Fig. 5. Potential energy as a function of the angle α between the H–O axis and the surface normal for OH at the short-bridge site on Ag(110). Definitions are given in the text.

Mulliken population studies show that the net charge transfer from the surface to OH is 0.74e, 0.42e, 0.62e and 0.58e at the short-bridge, threefold, long-bridge and fourfold on-top sites respectively. The bonding nature of OH on Ag(110) is similar to that of OH on Ag(100) discussed above. At the short-bridge site, the main OH 3σ bonding feature occurs at 13.68 eV, and the main OH 1π bonding features occur at 7.67 and 7.35 eV, as shown in Table 3. Considering that Koopman's theorem would place the σ and π levels deeper than the UPS measurements, the present results are in good agreement with the ARUPS assignments of 10–14 eV and around 8 eV for the 3σ and 1π bonding levels of OH adsorption on Ag(110) [24].

3.3. OH adsorption on Ag(111)

Table 5 shows the calculated adsorption energies, optimized geometries and HO–surface stretching frequencies for OH adsorbed at different sites on an Ag(111) surface. The calculated adsorption energies are 97.3 kcal mol^{-1}, 95.2 kcal mol^{-1} and 80.2 kcal mol^{-1} for OH adsorbed at the threefold, bridge and on-top sites

Table 5
Adsorption energies, optimized geometries and HO–surface stretching frequencies for OH adsorbed at different sites on the Ag(111) surface

Site[a]	E_{ads} (kcal mol^{-1})[b]	$R_{O-surface}$ (Å)[c]	R_{O-Ag} (Å)[c]	R_{O-H} (Å)[c]	HO–Ag stretch (cm^{-1})
On-top	80.2	2.242	2.242	0.941	307
Bridge	95.2	1.798	2.306	0.942	296
Threefold	97.3	1.719	2.395	0.943	277
Experiment.	–	–	–	–	300

[a] Adsorption sites are illustrated in Fig. 1a.
[b] Adsorption energy is defined as $E_{ads} = -[E(Ag_{10}OH) - E(Ag_{10}) - E(OH)]$ and calculated by the MP2 method. Positive values are exothermic.
[c] $R_{O-surface}$ is the perpendicular distance from oxygen to the Ag surface, and R_{O-Ag} is the corresponding distance from the oxygen nucleus to the nearest Ag nucleus. All the geometries are calculated by an HF optimization procedure except the assumption that the H–O molecular axis is perpendicular to the surface normal.

with O–surface perpendicular distances of 1.72 Å, 1.80 Å, and 2.24 Å respectively. The corresponding distances from O to the nearest Ag are also listed in Table 5. The HO–surface stretching frequencies are calculated to be 277 cm^{-1}, 296 cm^{-1} and 307 cm^{-1} for OH adsorbed at the threefold, bridge and on-top sites respectively. The experimental value of 300 cm^{-1} was assigned to OH on Ag(111) [20]. The calculations show that the energy difference between the bridge and threefold sites is only 2 kcal mol^{-1}. Thus, the two adsorption sites are competitive, and essentially no ordered OH overlayer will exist on the Ag(111) surface. Experimentally, an ordered c(2×2) LEED pattern and ordered ($1\times m$) ($m=1, 2, 3$) LEED patterns are observed for OH on Ag(100) [21] and Ag(110) [22,24] respectively, but no ordered OH LEED structures are found for Ag(111) [21].

The calculated adsorption energy for OH on Ag(111) is smaller than that for OH on Ag(110) and Ag(100). The reactivity for OH adsorption on silver surfaces is in the order Ag(110) > Ag(100) > Ag(111). The work functions of Ag(100), Ag(110), and Ag(111) surfaces are 4.61 eV, 4.52 eV, and 4.74 eV [47] respectively. The adsorption behavior of OH on Ag(111) is similar to that on Cu(111) [32] and Ni(111) [29]. All these theoretical studies [29,32] clarified the high-coordinated threefold site as the most stable adsorption site.

Fig. 6 shows the potential energy curve for tilting of OH adsorbed on Ag(111). For OH at the threefold and bridge sites the total energy increases when the H–O axis is tilted toward the surface, though the potential surfaces are very flat compared with those on Ag(100) shown in Fig. 2. The energy increase is only 1 kcal mol^{-1} even when the H–O axis is tilted 30° from the surface normal. For OH at the on-top site, the potential minimum is at $\alpha = 60°$, similar to that on Ag(100). Since the adsorption at the on-top site is much less stable than that at the bridge and threefold sites, OH does not remain adsorbed at the on-top site on Ag(111) at low coverage. The net charge

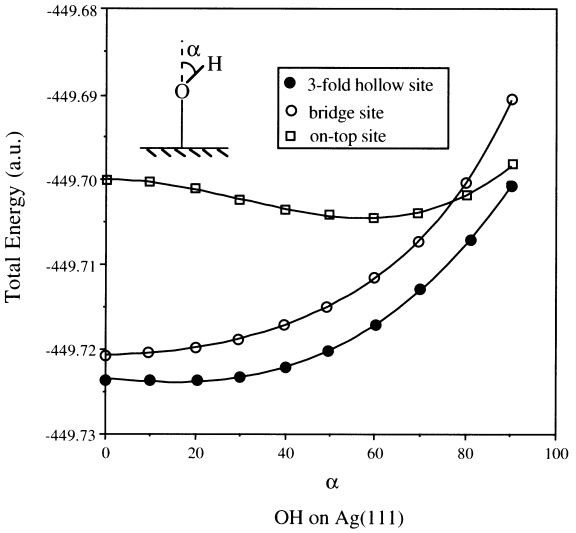

Fig. 6. Potential energy as a function of the angle α between the H–O axis and the surface normal for OH on Ag(111). Definitions are given in the text.

transfer from the surface to OH is calculated to be 0.78*e*, 0.55*e* and 0.47*e* for OH adsorbed at the on-top, bridge and threefold sites, which is similar to those for OH adsorbed on Ag(100) and Ag(110), and a similar bonding interaction is elucidated, as shown in Table 3.

4. Coadsorption of OH + OH on Ag(100)

In this section we investigate the coadsorption of two OH radicals on an Ag(100) surface, since several experimental studies have shown that OH can form ordered structures on Ag surfaces [21,22,24] and an ordered c(2 × 2) LEED structure was reported on Ag(100) [21]. Fig. 7 shows the optimized geometries, coadsorption energies, relative energies and adsorption energies of the second OH species for OH at several different sites on Ag(100). Coadsorption energy was defined as $E_{\mathrm{coads}}(2\mathrm{OH}) = -\{E[\mathrm{Ag_8(OH)_2}] - E(\mathrm{Ag_8}) - 2E(\mathrm{OH})\}$. The relative energies were calculated with respect to the coadsorption state of OH at the fourfold–fourfold sites, as shown in Fig. 7a.

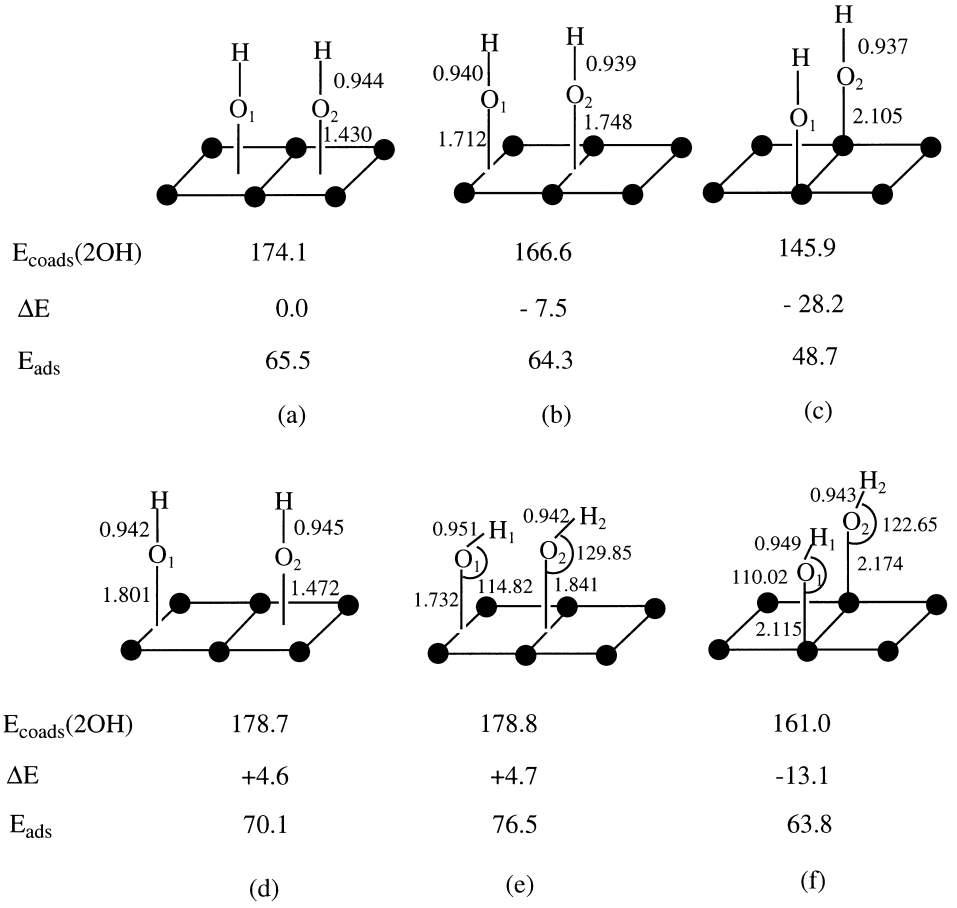

Fig. 7. Geometries, coadsorption energies, relative energies and adsorption energies of the second OH for OH coadsorption on an Ag(100) surface. (a) Fourfold–fourfold sites; (b) bridge–bridge sites; (c) on-top–on-top sites; (d) fourfold–bridge sites; (e) tilted geometry at the bridge sites; (f) tilted geometry at the on-top sites. The coadsorption energy is defined as $E_{\mathrm{coads}}(2\mathrm{OH}) = -\{E[\mathrm{Ag_8(OH)_2}] - E(\mathrm{Ag_8}) - 2E(\mathrm{OH})\}$. ΔE is the relative energy compared with (a). The adsorption energy of the second OH is defined as $E_{\mathrm{ads}} = -\{E[\mathrm{Ag_8(OH)_2}] - E(\mathrm{Ag_8O_2H}) - E(\mathrm{OH})\}$. Negative values are endothermic. Energy is in kilocalories per mole, bond lengths are in Ångströms and angles are in degrees.

The adsorption energy of the second OH was calculated as $E_{ads} = -\{E[Ag_8(OH)_2] - E(Ag_8O_1H) - E(OH)\}$.

Fig. 7a–d shows the coadsorbed vertical structures for OH on Ag(100). Coadsorption at the fourfold–bridge sites (Fig. 7d) has the largest adsorption energy, with the O–surface and O–H distances almost the same as those in the separate fourfold and bridge adsorption states. The O_1–O_2 separation is 4.35 Å. When coadsorptions occur at the fourfold (Fig. 7a), bridge (Fig. 7b) and on-top (Fig. 7c) sites, the O_1–O_2 distance decreases into 2.56 Å, the O–surface distances are slightly shorter than those for OH on a clean Ag(100) surface and they become less stable. These results imply that a repulsive interaction between the negatively charged coadsorbed OH exists when the HO···OH lateral distance is shortened. The adsorption energies of the second OH were calculated to be 70.1, 65.5, 64.3 and 48.7 kcal mol^{-1}, which are about two-thirds of those (108.6, 108.6, 102.3 and 97.2 kcal mol^{-1}) for OH adsorption on a clean Ag(100) surface. Although no experimental results are available for comparison, a BOC–MP study [54] of OH on Ni showed that the adsorption energy decreases as OH coverage increases, with values of 61 kcal mol^{-1}, 43 kcal mol^{-1} and 34 kcal mol^{-1} for OH surface coverage of $\Theta = 0$, 0.6 and 1.0 respectively. Coadsorption at the fourfold sites is more stable than that at the bridge and on-top sites, and shows that OH coadsorption at the nearest fourfold sites and the formation of an ordered OH adsorbed layer are possible on Ag(100).

As mentioned earlier, the O–H axis is found to be perpendicular to the surface at the fourfold site, and the tilted geometries are favorable for OH at the bridge and on-top sites on the clean Ag(100) surface. A similar trend is also obtained for the coadsorption of OH on Ag(100). At the fourfold sites the stable geometry is with the O–H axis perpendicular to the surface, as shown in Fig. 7a. On the other hand, the tilted geometries are much more favorable for OH coadsorbed at the bridge and on-top sites on Ag(100), as shown in Fig. 7e and 7. In these states, the O–H axis can tilt up to 70° toward the nearest oxygen, and they are 12.2 and 15.1 kcal mol^{-1} more stable than the corresponding vertical geometries shown in Fig. 7b and c. This means that the coadsorption structures in Fig. 7b and c are unlikely to occur even at higher OH coverage. In comparison with the bridge site, the on-top site is less favorable since it is 17.8 kcal mol^{-1} more unstable. The tilted coadsorption at bridge sites has the same stability as that shown in Fig. 7d and likely leads to a surface disproportionation reaction for OH on Ag(100).

The relative energy shown in Fig. 7 also helps us to understand the surface migration of OH on Ag(100). Moving the OH from the bridge site (Fig. 7d) to the nearest fourfold site (Fig. 7a) decreases the adsorption energy by 4.6 kcal mol^{-1}, whereas moving the OH from the fourfold sites (Fig. 7d) to the tilted bridge sites (Fig. 7e) increases the adsorption energy by 0.1 kcal mol^{-1}. Coadsorption at the bridge and on-top sites with the H–O axis perpendicular to the surface increases the total energy by 7.5 kcal mol^{-1} and 28.2 kcal mol^{-1} respectively. The tilted on-top structure (Fig. 7f) is 13.1 kcal mol^{-1} more unstable than the vertical coadsorption at the fourfold sites. Thus, the favorable coadsorptions are those shown in Fig. 7a, d and e. It is noted that although both coadsorption and surface migration phenomena are still difficult to describe quantitatively, the present calculations do give some information on these problems.

Fig. 8 shows the geometries and energies for OH coadsorbed on the Ag_{11} model. The Ag_{11} model should be more reasonable to describe the bridge coadsorption site. Two adsorbed OH species are assumed to be in the same plane in Fig. 8a–c. The results shown in Fig. 8a–c will then be comparable with those shown in Fig. 7b, e and d. It is shown that the coadsorption energies are decreased almost by a constant 4–5 kcal mol^{-1} on the Ag_{11} model. Since the adsorption energy for OH at the bridge site is decreased only by 1 kcal mol^{-1}, the decrease reflects a lower adsorption energy for the second OH species. On the other hand, the relative energy differences are very small: 10.9 kcal mol^{-1} (Fig. 8b versus Fig. 8a) versus 12.2 kcal mol^{-1} (Fig. 7e versus Fig. 7b) and 10.5 kcal mol^{-1} (Fig. 8c versus Fig. 8a) vs. 12.1 kcal mol^{-1} (Fig. 7d versus Fig. 7b). This means that the results based on the Ag_8 model are

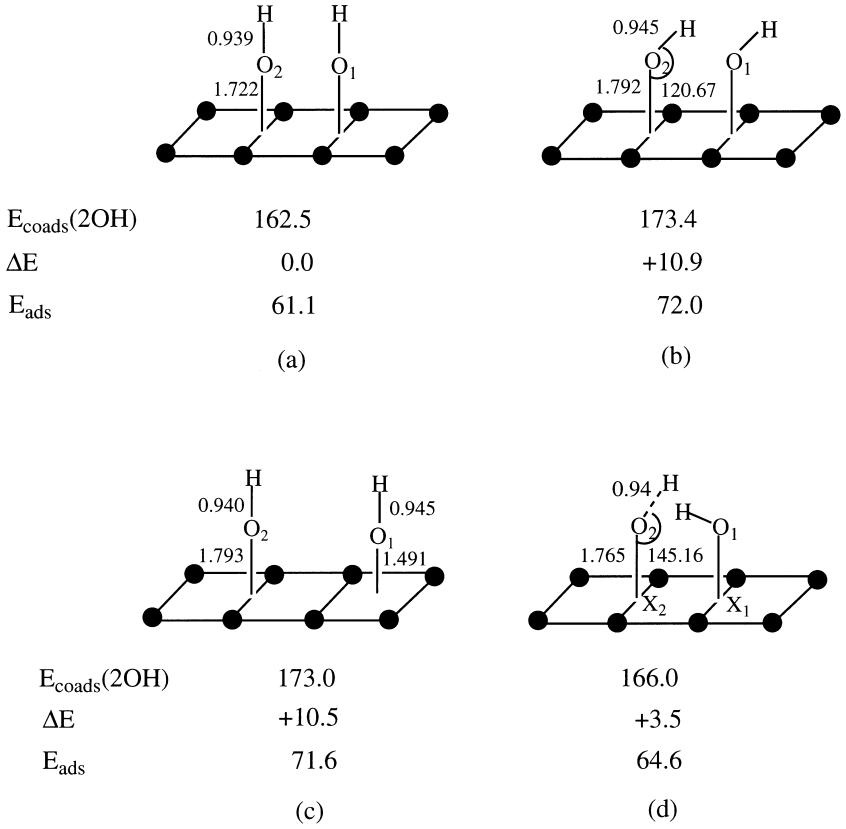

Fig.8. Geometries, coadsorption energies, relative energies and adsorption energies of the second OH radical for OH on the Ag_{11} cluster modeled Ag(100) surface. (a) Bridge–bridge sites; (b) tilted geometry at the bridge sites (I); (c) fourfold–bridge sites; (d) tilted geometry at the bridge sites (II). The coadsorption energy is defined as $E_{coads}(2OH) = -\{E[Ag_{11}(OH)_2] - E(Ag_{11}) - 2E(OH)\}$. ΔE is the relative energy compared with (a). The adsorption energy of the second OH is defined as $E_{ads} = -\{E[Ag_{11}(OH)_2] - E(Ag_{11}O_2H) - E(OH)\}$. Energy is in kilocalories per mole, bond lengths are in Ångströms and angles are in degrees.

acceptable. Fig. 8d shows another coadsorption geometry in which the hydrogen is out of the $O_1O_2X_1X_2$ plane in order to have the largest freedom in the optimization, but the dihedral angle is only 0.2° in our calculation. The coadsorption shown in Fig. 8d is 3.5 kcal mol^{-1} more stable than the vertical geometry shown in Fig. 8a; however, it is 7.4 kcal mol^{-1} more unstable than that shown in Fig. 8b and seems not to be the most possible coadsorption species. It is noted that the Ag_{11} cluster may not be an appropriate model for fourfold coadsorption as we cannot get a reasonable geometry in our optimization calculation. Therefore, the discussions for the coadsorption and reaction at the fourfold sites are limited in the Ag_8 model calculations and compared with those at the bridge sites on the same model.

5. Mechanism of the disproportionation reaction of OH on Ag(100): $2OH \rightarrow H_2O + O$

Disproportionation of OH to form gas-phase H_2O [Eq.(2)] is an important practical surface reaction in heterogeneous catalysis. Although the reaction expressed by Eq.(2) seems to be extremely simple, the mechanistic details have not been clarified despite many experimental efforts [1–26], and

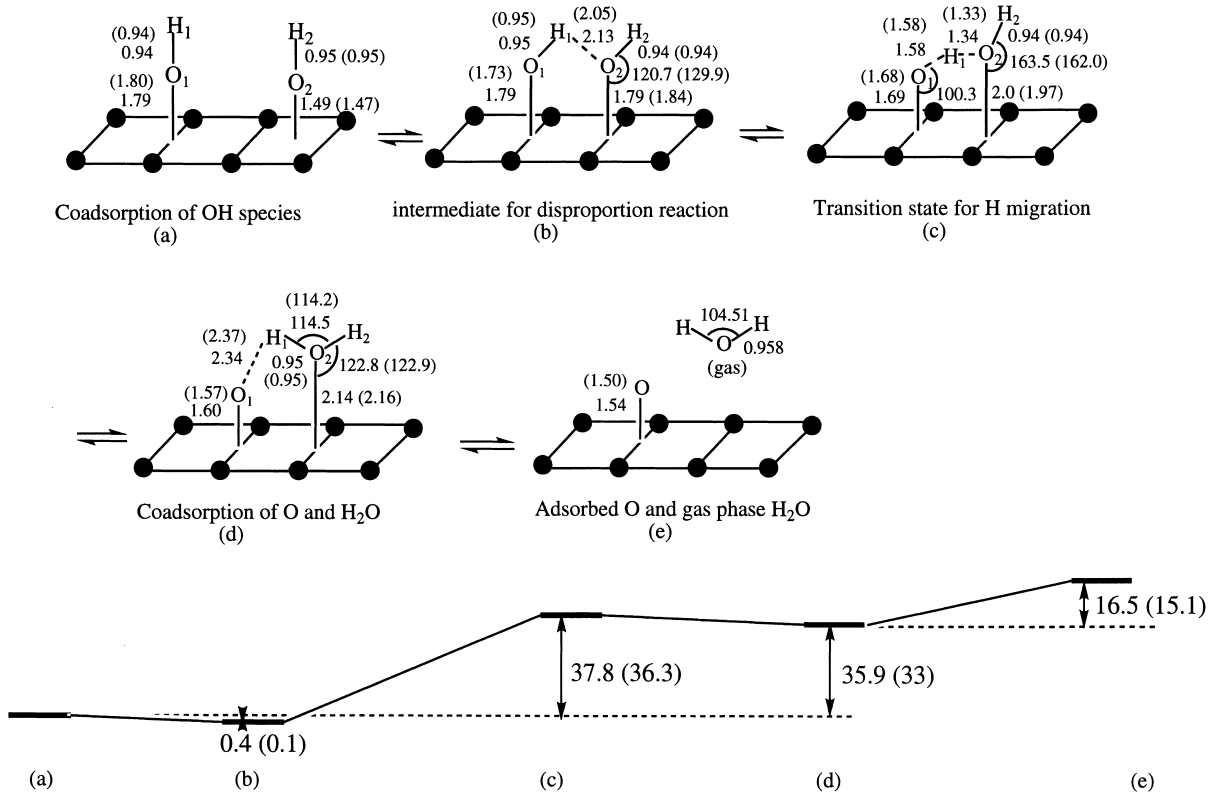

Fig. 9. Geometries and energy diagrams for the surface disproportionation of $2OH \rightarrow H_2O + O$ at the bridge sites on an Ag(100) surface. Energy is in kilocalories per mole, bond distance is in Ångströms and bond angles are in degrees. The optimized geometries were obtained by the HF optimization procedure, and the energy diagrams were calculated by the MP2 method. The energies and geometries calculated by the Ag_8 cluster are given in parentheses.

there has been no theoretical study, perhaps due to the lack of a suitable method for describing the surface OH in the reaction process. In our previous studies [41–46], a series of surface reaction mechanisms were clarified using the DAM [34–36]. Here, we investigate the mechanism of the surface disproportionation reaction of OH on an Ag(100) surface.

Two reaction pathways, one is at the bridge sites (Fig. 9) and another is at the fourfold sites (Fig. 10), were studied. For the reaction at the bridge sites, essentially two equivalent bridge sites should be simulated; the Ag_{11} model shown in Section 4 is used. For comparison, the results on the Ag_8 model are also shown in Fig. 9. It is found that the results are very similar between the Ag_8 and Ag_{11} cluster models and, therefore, the discussions and conclusions are the same. The Ag_8 cluster is then used for the reaction path study at the fourfold sites shown in Fig. 10. The reaction coordination is selected to be in the plane that is vertical to the surface above the bridge and fourfold sites. The geometry and energy surface for the H migration reaction are studied and a C_s symmetry is held in the reaction paths. Fig. 9 shows the geometry and energy diagram for the reaction at the bridge sites. The reaction proceeds from left to right, and the energy scale is in kilocalories per mole relative to the left coadsorption state of OH at the fourfold–bridge sites. Migration of OH from the fourfold to the bridge site leads to the formation of an intermediate state. In this state, two inclined OH are coadsorbed at the bridge sites and it is exothermic by

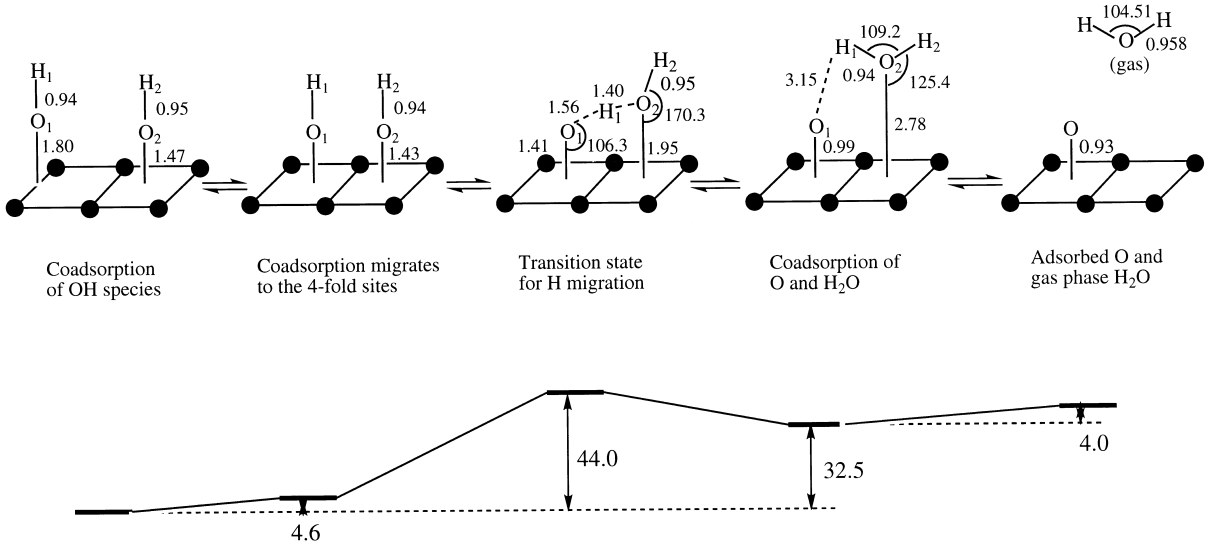

Fig. 10. Geometries and energy diagrams for the surface disproportionation of $2OH \rightarrow H_2O + O$ at the fourfold sites on Ag(100) surface. Energy is in kilocalories per mole, bond distance is in Ångströms and bond angles are in degrees. The optimized geometries were obtained by the HF optimization procedure, and the energy diagrams were calculated by the MP2 method.

0.4 kcal mol^{-1}. The $H_1 \cdots O_2$ distance is shortened to 2.13 Å. The H_1–O_2 distance decreases from 2.13 to 1.34 Å in the TS, and then to 0.95 Å in the next intermediate state. Meanwhile, the O_1–H_1 distance increases from 0.95 to 1.58 Å, and then to 2.34 Å, which reflects a reasonable H migration reaction path. On the other hand, the O_1–surface distance changes from 1.79 to 1.69 Å and then to 1.60 Å, while the O_2–surface distance changes from 1.79 to 2.0 Å and then to 2.14 Å, which reflects the surface disproportionation of OH on Ag(100). This reaction path was calculated to have an energy barrier of 37.8 kcal mol^{-1}, and to be endothermic by 35.9 kcal mol^{-1}. The energy levels are 36.3 kcal mol^{-1} and 33 kcal mol^{-1} respectively on the Ag_8 model.

The reaction path at the fourfold sites is shown in Fig. 10. In this path, migration of OH from the bridge to the fourfold site leads a coadsorption state of OH at the fourfold sites and an energy loss of 4.6 kcal mol^{-1}. The $H_1 \cdots O_2$ distance is 3.04 Å. The energy level at the TS is calculated to be 44 kcal mol^{-1} higher than the coadsorption state at the fourfold–bridge sites, and it is 7.7 kcal mol^{-1} higher than that of the TS state shown in Fig. 9. Coadsorption of oxygen and water at the fourfold sites is 11.5 kcal mol^{-1} more stable than the TS. Although Fig. 9 also shows a reasonable disproportionation reaction path, the bridge site reaction path shown in Fig. 9 has the lower energy barrier and is an easier path towards disproportionation. The reason for the energy difference between bridge and fourfold site reaction paths is due to the difference of the coadsorption states; the former has the deformed geometry with the larger adsorption energy and the shorter $H_1 \cdots O_2$ distance and, therefore, it likes to be the precursor for the disproportionation reaction.

The results shown in Figs. 9 and 10 also reflect the site dependence for oxygen adsorption on clean Ag(100) and H_2O adsorption on an oxygen-covered Ag(100) surface. Oxygen adsorbed at the fourfold site is 11.6 kcal mol^{-1} more stable than that at the bridge site. The adsorption energy for H_2O at the bridge oxygen-covered Ag(100) was calculated to be 15.1 kcal mol^{-1} by the Ag_8 cluster model, while it is 4.0 kcal mol^{-1} at the fourfold oxygen-covered Ag(100). The adsorption energy of H_2O on a clean silver surface is estimated to be approximately 10 kcal mol^{-1} [21,22]. The energy levels of the coadsorbed oxygen and H_2O at the bridge and fourfold sites on the Ag_8 cluster are

Table 6
Mulliken charge for the $Ag_{11}(OH)_2$ adclusters in the reaction pathway of $2OH \rightarrow H_2O + O$ shown in Fig. 9. Mulliken charges are given relative to neutral atoms

	Coads. of OH species	Intermediate	TS for H migration	Coads. of O and H_2O	Oxygen ads. and H_2O (gas)
Ag_1	0.176	0.244	0.133	0.206	0.016
Ag_2	0.176	0.244	0.133	0.206	0.016
Ag_3	−0.046	−0.112	−0.113	−0.168	−0.122
Ag_4	−0.046	−0.112	−0.113	−0.168	−0.122
Ag_5	0.131	0.088	0.017	−0.138	−0.083
Ag_6	0.131	0.088	0.017	−0.138	−0.083
Ag_7	−0.067	−0.086	−0.031	−0.067	−0.004
Ag_8	−0.067	−0.086	−0.031	−0.067	−0.004
Ag_9	−0.142	−0.191	−0.183	−0.169	−0.128
Ag_{10}	0.040	0.054	0.074	−0.001	0.080
Ag_{11}	−0.184	−0.126	−0.182	−0.028	−0.175
O_1	−0.941	−0.768	−0.612	−0.542	−0.393
H_1	0.318	0.378	0.361	0.401	0.338
O_2	−0.806	−0.942	−0.814	−0.686	−0.677
H_2	0.327	0.327	0.343	0.346	0.338

Table 7
Net charge for the $Ag_8(OH)_2$ adclusters in the reaction pathway of $2OH \rightarrow H_2O + O$ shown in Fig. 10. Mulliken charges are given relative to neutral atoms

	Coads. of OH species	Coads. of OH at fourfold sites	TS for H migration	Coads. of O and H_2O	Oxygen ads. and H_2O (gas)
Ag_1	0.066	0.090	−0.074	−0.008	−0.076
Ag_2	0.066	0.090	−0.074	−0.008	−0.076
Ag_3	−0.041	−0.018	−0.058	−0.174	−0.198
Ag_4	−0.041	−0.018	−0.058	−0.174	−0.198
Ag_5	0.095	−0.018	0.029	0.012	−0.014
Ag_6	0.095	−0.018	0.029	0.012	−0.014
Ag_7	−0.140	−0.095	−0.095	−0.166	−0.002
Ag_8	−0.035	−0.095	−0.060	−0.159	−0.156
O_1	−0.776	−0.778	−0.692	−0.363	−0.268
H_1	0.322	0.319	0.325	0.339	0.338
O_2	−0.926	−0.778	−0.561	−0.625	−0.677
H_2	0.311	0.319	0.289	0.339	0.338

almost the same. The site dependence of H_2O on an oxygen-covered Ag(100) can be understood by the geometrical difference at the coadsorption states. In the bridge site coadsorption state the H–O–H angle increases from 104.5° (gas phase) to 114.2° and the O–surface distance is 2.16 Å, whereas the H–O–H angle increases from 104.5 to 109.2° and the O–surface distance is as large as 2.78 Å at the coadsorbed fourfold sites. The geometry of the adsorbed H_2O at the fourfold site is little changed compared with the gas-phase state, and the adsorption is then weaker than that at the bridge site. The net charges for each reaction state in the reaction pathways are shown in Tables 6 and 7. The electronic state of the Ag cluster is little changed. Changes take place at the adsorbed OH side, especially the change of the adsorbed oxygen (O_1) species to the adsorbed OH species.

The present calculations provide clear information regarding the disproportionation of OH on an Ag(100) surface. OH can be coadsorbed on Ag(100), as shown in Section 4 and in this section.

At high OH coverages, OH can migrate to the nearest adsorption site without a large energy barrier. An inclined OH adsorption species is expected, and is also the most important precursor for the disproportionation reaction. The reaction takes place between the nearest H and O atoms, and one H migrates to the nearest O, leading to the formation of coadsorbed H_2O. H_2O can then desorb from the surface to the gas phase at a higher temperature. Note that the results shown in Figs. 9 and 10 show not only the reaction path for the disproportionation of OH, but also the reaction path for the decomposition [Eq. (1)] of H_2O on an oxygen-covered Ag(100) surface. The reverse reaction [Eq. (1)] can proceed much easier than the disproportionation of OH [Eq. (2)] on Ag(100), based on our calculations and other experimental evidence.

6. Conclusions

In this study, we examined the adsorption and surface disproportionation of OH on silver surfaces. We performed both ab initio HF and MP2 calculations using the DAM, which involves the interaction between bulk metal and admolecules while considering electron transfer and image force correction.

OH binds strongly to clean Ag surfaces. The adsorption energies were calculated to be 118.3 kcal mol^{-1} at the short bridge site on Ag(110), 108.6 kcal mol^{-1} at the fourfold hollow site on Ag(100), and 97.3 kcal mol^{-1} at the threefold hollow site on Ag(111). A high-coordination site is generally favorable for OH adsorption on Ag surfaces. The reactivity of Ag surfaces for OH adsorption is in the order of Ag(110) > Ag(100) > Ag(111).

On Ag(100) and Ag(111) surfaces, the OH adsorbed at the high-coordination hollow site with its molecular axis preferentially perpendicular to the surface. However, there is only a small difference in energy between the bridge and hollow sites, and the H–O axis can tilt up to 30° with almost no change in energy on Ag(111). On the other hand, the properties of OH adsorption on Ag(110) are slightly different from those on Ag(100) and Ag(111), in that OH is adsorbed at the short bridge site with the H–O axis tilting about 50° from the surface normal, and the azimuthal orientation is in the [001] direction.

The strong interactions of OH with silver are due to the electron transfer from the surface to OH. The net charge transfer was calculated to be about 0.78*e*, 0.64*e* and 0.43*e* for OH adsorbed at the on-top, bridge and hollow sites on Ag(100) respectively. The Ag 4d states play an important role in the adsorption interaction with OH. In the adsorption states the OH 1π orbital mixes strongly with Ag 4d states, and to a lesser extent with 5s states, leading to bonding and anti-bonding levels among and above the metal d bands respectively, whereas the OH 3σ orbital also mixes strongly with Ag 4d states, leading to bonding and anti-bonding levels below and above the metal d bands respectively. The net effect is a charge transfer from the surface to the OH 1π orbital.

Coadsorption of OH at the nearest fourfold sites on Ag(100) occurs steadily and the H–O axis is perpendicular to the surface, suggesting a possible ordered surface OH overlayer. The inclined OH structure is favorable for the coadsorption of OH at bridge sites, and high reactivity with regard to OH disproportionation is expected in this state. The migration of OH on Ag(100) is not difficult owing to the small energy barrier.

The disproportionation of OH to form H_2O on Ag(100) is endothermic. The activation energy for OH disproportionation at the bridge sites is 37.8 kcal mol^{-1}, and is endothermic by 35.9 kcal mol^{-1} in the H_2O coadsorption state. The reverse reaction, H_2O decomposition, occurs much more readily than the disproportionation reaction of OH on an Ag(100) surface.

Acknowledgements

Some calculations were performed using the computers at the Institute for Molecular Science. Part of this study was supported by a Grant-in-Aid for Scientific Research from the Japanese Ministry of Education, Science, and Culture, and by a grant from the Kyoto University VBL Project.

References

[1] P.R. Norton, in: D.A. King, D.P. Woodruff (Eds.), The Chemical Physics of Solid Surfaces and Heterogeneous Catalysis, vol. 3, Elsevier, Amsterdam, 1990.
[2] D.S. Newsome, Catal. Rev. Sci. Eng. 21 (1980) 275.
[3] J.T. Keiser, M.A. Hoffbauer, M.C. Lin, J. Phys. Chem. 89 (1985) 2635.
[4] F.P. Netzer, T.E. Madey, Phys. Rev. Lett. 47 (1981) 928.
[5] C. Benndorf, C. Nöbl, T.E. Madey, Surf. Sci. 138 (1984) 292.
[6] S. Ljunström, J. Hall, B. Kasemo, A. Rosèn, T. Wahnström, J. Catal. 107 (1987) 548.
[7] C. Nyberg, P. Uvdal, J. Chem. Phys. 84 (1986) 4631.
[8] L.C. Anderson, C.E. Mooney, J.H. Lunsford, Chem. Phys. Lett. 196 (1992) 445.
[9] P.A. Thiel, F.M. Hoffmann, W.H. Weinberg, J. Chem. Phys. 75 (1981) 5556.
[10] K. Kretschmar, J.K. Sass, A.M. Bradshaw, S. Holloway, Surf. Sci. 115 (1982) 183.
[11] G.T. Fujimoto, G.S. Selwyn, J.T. Kelser, M.C. Lin, J. Phys. Chem. 87 (1983) 1906.
[12] L.V. Novakoski, D.S.Y. Hsu, J. Chem. Phys. 92 (1990) 1999.
[13] C.E. Mooney, L.C. Andeerson, J.H. Lunsford, J. Phys. Chem. 95 (1991) 6070.
[14] W.R. Williams, C.M. Mark, L.D. Schmidt, J. Phys. Chem. 96 (1992) 5922.
[15] V.J. Kwasniewski, L.D. Schmidt, J. Phys. Chem. 96 (1992) 5931.
[16] C.M. Mark, L.D. Schmidt, Chem. Phys. Lett. 178 (1991) 358.
[17] M.P. Zum Mallen, W.R. Williams, L.D. Schmidt, J. Phys. Chem. 97 (1993) 625.
[18] K. Bange, D.E. Grider, T.E. Madey, J.K. Sass, Surf. Sci. 137 (1984) 38.
[19] R. Brosseau, M.R. Brustein, T.H. Ellis, Surf. Sci. 294 (1993) 243.
[20] A.F. Carley, P.R. Davies, M.W. Roberts, K.K. Thomas, Surf. Sci. 238 (1990) L467.
[21] M. Klaua, T.E. Madey, Surf. Sci. 136 (1984) L42.
[22] K. Bange, T.E. Madey, J.K. Sass, E.M. Stuve, Surf. Sci. 183 (1987) 334.
[23] E.M. Stuve, R.J. Madix, B.A. Sexton, Surf. Sci. 111 (1981) 11.
[24] M. Canepa, P. Cantini, L. Mattera, E. Narducci, M. Salvietti, S. Terreni, Surf. Sci. 322 (1995) 271.
[25] M.A. Barteau, R.J. Madix, in: D.A. King, D.P. Woodruff (Eds.), The Chemical Physics of Solid Surfaces and Heterogeneous Catalysis, vol. 4, Elsevier, Amsterdam, 1982.
[26] I.E. Wachs, R.J. Madix, Surf. Sci. 76 (1978) 531.
[27] A.B. Anderson, Surf. Sci. 105 (1981) 159.
[28] C.W. Bauschlicher Jr., Int. J. Quantum Chem. S20 (1986) 563.
[29] H. Yang, J.L. Whitten, J. Phys. Chem. B 101 (1997) 4090.
[30] H. Yang, J.L. Whitten, Surf. Sci. 223 (1989) 131.
[31] H. Yang, J.L. Whitten, Surf. Sci. 370 (1997) 136.
[32] K. Hermann, M. Witko, L.G.M. Pettersson, P. Siegbahn, J. Chem. Phys. 99 (1993) 610.
[33] E.A. Carter, W.A. Goddard III, Surf. Sci. 209 (1989) 243.
[34] H. Nakatsuji, J. Chem. Phys. 87 (1987) 4995.
[35] H. Nakatsuji, H. Nakai, Y. Fukunishi, J. Chem. Phys. 95 (1991) 640.
[36] H. Nakatsuji, Prog. Surf. Sci. 54 (1997) 1.
[37] H. Nakatsuji, R. Kuwano, H. Morita, H. Nakai, J. Mol. Catal. 82 (1993) 211.
[38] H. Nakatsuji, H. Nakai, Chem. Phys. Lett. 174 (1990) 283.
[39] H. Nakatsuji, H. Nakai, Can. J. Chem. 70 (1992) 404.
[40] H. Nakatsuji, H. Nakai, J. Chem. Phys. 98 (1993) 2423.
[41] H. Nakatsuji, H. Nakai, K. Ikeda, Y. Yamamoto, Surf. Sci. 384 (1997) 315.
[42] H. Nakatsuji, K. Takahashi, Z.M. Hu, Chem. Phys. Lett. 277 (1997) 551.
[43] H. Nakatsuji, Z.M. Hu, H. Nakai, Int. J. Quantum Chem. 65 (1997) 839.
[44] Z.M. Hu, H. Nakai, H. Nakatsuji, Surf. Sci. 401 (1998) 371.
[45] H. Nakatsuji, Z.M. Hu, H. Nakai, K. Ikeda, Surf. Sci. 387 (1997) 328.
[46] Z.M. Hu, K. Takahashi, H. Nakatsuji, submitted to Surf. Sci.
[47] R.C. Weast, M.J. Astle, W.H. Beyer, Handbook of Chemistry and Physics, CRC Press, Florida, 1984, p. E-76.
[48] M.J. Frish, G.W. Trucks, H.B. Schlegel, P.M.W. Gill, B.G. Johnson, M.A. Robb, J.R. Cheeseman, T.A. Keith, G.A. Petersson, J.A. Montgomery, K. Raghavachari, M.A. Al-Laham, V.G. Zakrzewski, J.V. Ortiz, J.B. Foresman, J. Cioslowski, B.B. Stefanov, A. Nanayakkara, M. Challacombe, C.Y. Peng, P.Y. Ayara, W. Chen, M.W. Wong, J.L. Andres, E.S. Replogle, R. Gomperts, R.L. Martin, D.J. Fox, J.S. Binkley, D.J. Defrees, J. Baker, J.P. Stewart, M. Head-Gordon, C. Gonzalez, J.A. Pople, Gaussian 94 (Revision E.2), Gaussian, Inc., Pittsburgh, PA, 1995.
[49] P.J. Hay, W.R. Wadt, J. Chem. Phys. 82 (1985) 270.
[50] S. Huzinaga, J. Chem. Phys. 42 (1965) 1293.
[51] T.H. Dunning Jr,, J. Chem. Phys. 53 (1970) 2823.
[52] T.H. Dunning Jr, P.J. Hay, in: H.F. Schaeffer (Ed.), Modern Theoretical Chemistry, vol. 3, Plenum, New York, 1977.
[53] S. Huzinaga, J. Andzelm, M. Kiobukowski, E. Radzio-Anzelm, Y. Sakai, H. Tatewaki, Gaussian basis sets for molecular calculations, Physical Science Data, vol. 16, Elsevier, Amsterdam, 1984, p. 23.
[54] E.M. Patrito, P.P. Olivera, H. Sellers, Surf. Sci. 306 (1994) 447.